Monolithically Integrable Si-Compatible Light Sources

Jesús Alarcón-Salazar, Liliana Palacios-Huerta,
Alfredo Abelardo González-Fernández,
Alfredo Morales-Sánchez and
Mariano Aceves-Mijares

Additional information is available at the end of the chapter

Abstract

On the road to integrated optical circuits, the light emitting device is considered the bottleneck preventing us from arriving to the fully monolithic photonic system. While the development of silicon photonics keeps building momentum, the indirect bandgap nature of silicon represents a major problem for obtaining an integrated light source. Novel nanostructured materials based on silicon, such as silicon-rich oxide (SRO) containing silicon nanoparticles, present intense luminescence due to quantum phenomena. Using this material, electroluminescent devices have already been fabricated and even integrated in monolithic photonic circuits by fully complementary metal oxide semiconductor (CMOS) compatible techniques, opening the door to seamless electronic and photonic integration. The present work discusses some of the strategies used to improve the performance of SRO-based electroluminescent devices fully compatible with CMOS technology. Results from the characterization of devices obtained using different approaches are presented and compared.

Keywords: silicon-rich oxide, silicon nanoparticles, light emitting capacitor, photonic system, monolithic integration

1. Introduction

There are many research groups devoting their efforts to contribute to the development of a fully integrated photonic lab-on-a-chip (LOC) that can take advantage of the use of silicon (Si) as the main material. These are, among others, large availability and low cost of the material, a very well-established fabrication and testing ecosystem, the existence of a fabless model, very large chip fabrication volumes and yields, the possibility of testing using parallel

IntechOpen

systems, seamless integration with electronics, etc. All these advantages have driven a significant advancement in the past years regarding the development of Si-based LOC systems and, in particular, in silicon photonics. However, there still are important barriers to overcome that have prevented the transition from research to industrialization.

One of the most important limitations to achieve the goal of a monolithic integrated photonic system is the indirect band gap nature of silicon, which impedes the availability of light sources in the complementary metal oxide semiconductor (CMOS) technology. Aside from the integrated light emitting device, most of the rest of the problems regarding Si photonics have been solved, being its lack virtually of the only thing separating us from making monolithic Si-based LOC technology.

Depending on the application, the light source problem can be tackled in different manners. In the specific case of biophotonic applications where visible light is preferred [1], the silicon-rich oxide (SRO) or off stoichiometric oxide can be used to obtain light emitting capacitors (LECs). The SRO-based LECs emit almost in all the visible light range, and they are totally silicon compatible [2]. In fact, the integration of a light source, waveguide, and a sensor has already been theoretically and experimentally demonstrated using standard CMOS technology [3, 4].

The active material in a LEC is a SRO film, which can be obtained implanting Si ions into thermally grown silicon dioxide or using a variety of chemical vapor deposition (CVD) techniques. One of the most popular of the latter is the low-pressure CVD (LPCVD), which is a simple way to produce SRO with different silicon excesses [5, 6]. SRO-LPCVD is characterized by the ratio R_0, defined as

$$R_0 = \frac{P_{N_2O}}{P_{SiH_4}}$$

(1)

where P_{N_2O} and P_{SiH_4} are the partial pressures of the nitrous oxide and silane gases, respectively. Under this equation, $R_0 = 3$ produces SRO films with 17% atomic silicon excess, while $R_0 > 100$ produces stoichiometric oxide. R_0 values between 20 and 30 produce SRO with silicon excess between 4 and 5 at.%, which delivers a luminescent material, but with relatively poor electrical conductivity. On the other hand, SRO with $R_0 = 10$ or less presents a lower light emission and higher conductivity than those of the former.

Aside from the SRO-based LECs, there are very few reports on totally Si-compatible integrated photonic circuits, most of which use reverse biased PN junctions as the light source [7–9]. Other proposed solutions include the use of phosphorus doped germanium heterojunctions [10], the coupling to the photonic circuit of optical fibers pig-tailed to lasers [11], or the hybrid approximation, in which external nonsilicon sources such as III–V reflective semiconductor optical amplifiers (RSOAs) are used [12]. All the previous lack the possibility of taking advantage of the current techniques used for the massive production of silicon-integrated circuits (ICs). Finally, another approach uses the implantation of rare-earth elements into silicon oxide to produce light emission in the infrared communication region [13]. Again, such technique is not compatible with the standard silicon IC technology.

Then, SRO-based LECs present themselves as the most promising solution to a fully IC-compatible integrated photonic circuit including the three basic elements, i.e., emitter, waveguide, and detector, as demonstrated in [4]. However, at this point, they work in the edge of electric breakdown and consume larger power than that needed to comply with IC strict standards. Therefore, SRO-based LECs require new strategies or different approaches to improve their performance.

In this work, we review the fabrication and performance of LECs, fabricated by our research group, that use different substrate treatments and a variety of SRO compositions and configurations, as means of discussing the strategies to improve the behavior of these devices.

2. Experimental procedure

SRO-based LECs were fabricated using different structures and conditions, namely, SRO monolayers on polished Si-wafers, SRO monolayers on textured Si substrates, and SRO multilayers (MLs) with gradual and abrupt silicon excess. For reference, LECs with single SRO films and SRO in a multilayered structure will be labeled as S-LEC and M-LEC, respectively. The standard fabrication process used is completely compatible with the CMOS technology. For textured Si substrates, the reactive ion etching (RIE) process was used. In this process, Ar and SF_6 in proportion of 7:3 and power of 300 W were set to roughening surface during 1 min, resulting in conical structures over the surface with a roughness and peak density of 4.0 ± 0.2 nm and 3.7×10^{10} cm^{-2}, respectively.

SRO films (mono- or multilayers) were deposited at 720°C, on N-type or P-type silicon substrates ((100)-oriented) with low resistivity (between 1 and 10 $\Omega \times$ cm) by LPCVD and using the flow ratio (R_0) between N_2O and SiH_4 to vary the silicon excess. R_0 values of 5, 10, 20, 25, and 30 have been used to obtain different silicon excesses. Subscript of SRO labels indicates the R_0 parameter. After deposition, SRO films were thermally annealed at 1100°C for 3 h in nitrogen atmosphere in order to activate their photoluminescent (PL) emission.

For electrical and electroluminescent studies, metal insulator semiconductor (MIS)-like devices were fabricated. A semitransparent n$^+$ polycrystalline silicon (poly) gate was deposited onto the SRO film by LPCVD. After a photolithography process step, different shaped gates were defined. The backside contacts were obtained by the evaporation of an aluminum layer with thicknesses between 0.6 and 1 µm. Finally, the devices were thermally annealed at 480°C in forming gas in order to assure ohmic contacts.

The thickness of all samples, including multilayer structures, was measured using a null Gaertner L117 null ellipsometer with a He-Ne laser of 632.8 nm wavelength. PL spectra were obtained using a Horiba Yvon Fluoromax-3 spectrometer at room temperature; all the films were excited with UV radiation. Optical filters were used in order to guarantee the wavelength of the excitation beam. For electrical and electroluminescent studies, a source meter Keithley model 2400 was used. Electroluminescence (EL) spectra were obtained by biasing the devices with a constant DC voltage and measuring the emitted light by means of

an optical fiber normally aligned to the poly gate surface and connected to the Fluoromax 3 spectrometer. The optical power from the emitted light was measured with a 1400 IL radiometer connected to an UV-VIS GaAsP detector placed in front of the gate. Images from EL were obtained using a digital photographic camera. More specific details of the different characteristics of the studied LECs are addressed in Sections 3.1–3.3.

3. Results and discussion

3.1. SRO monolayers

This section shows the electro-optical properties of SRO films deposited on N-type silicon substrates using R_0 values of 20 (SRO_{20}) and 30 (SRO_{30}) and thicknesses of 70.1 ± 2.3 and 119.3 ± 4.9 nm, respectively. LECs with square-shaped poly gates of 4 mm^2 area and 400 nm thick were defined. To obtain PL spectra, the SRO samples (without poly gate) were excited using a 290 nm radiation.

The R_0 parameter is determinant in the structural, compositional, electrical, and light emitting characteristics of the SRO [14]. Red and blue electroluminescent devices have been obtained using R_0 = 20 and 30, respectively. **Figure 1** shows PL and EL spectra of S-LEC$_{20}$ and S-LEC$_{30}$. There, it is possible to see that both samples emit red PL, but changes in the emission wavelength are obtained with electrical stimulation, especially for SRO_{30}, where a blue EL band is observed with the main peak at 468 nm. A long spectral shift, blue shift, of almost ~227 nm is observed between the EL and PL bands of the SRO_{30} films (blue dash line). LECs with SRO_{20} films emit a broad EL spectrum in the red region (713 nm), as observed in **Figure 1**. An additional EL peak of low intensity is also observed at 468 nm. There exists also a blue spectral shift of the EL with respect to the PL spectrum in SRO_{20} films but much smaller, remaining in the red side of the spectrum (red dash line), which could indicate that the same luminescent centers are involved in both luminescence types. In both SROs, the EL emission is bright and
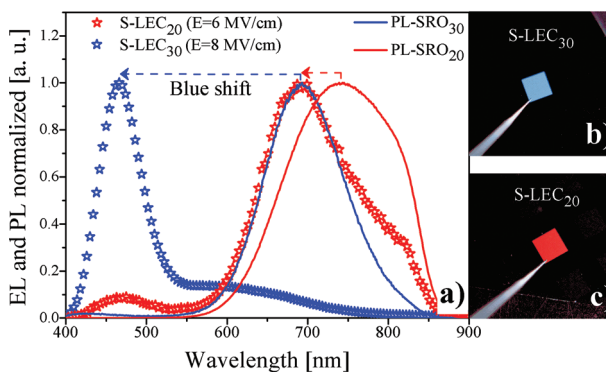

Figure 1. (a) PL (solid line) and EL (symbols) spectra of S-LEC$_{20}$ and S-LEC$_{30}$. Images of (b) blue (S-LEC$_{30}$) and (c) red (S-LEC$_{20}$) bright emission.

observable to the naked eye, as shown in **Figure 1(b)** and **(c)**. Notably, this intense EL is emitted in the whole area of the LEC devices. As expected, the intensity of the full-area emission increases as the applied electric field is increased [15].

Different authors have attributed the spectral shift between PL and EL to three different origins: defects in the SiO_2 matrix, band filling when bipolar injection is achieved, and silicon nanocrystal (Si-nc) size selection by the injected electrons energy [16–18]. In our case, the red EL observed in S-LEC$_{20}$ is ascribed to surface defects on the Si-ncs, which have been observed by transmission electron microscopy (TEM) [14]. While the blue EL in SRO$_{30}$ devices is consistent with the emission related to defects such as oxygen defect centers (ODC), non-bridging oxygen hole centers (NBOHC), and E'$_\delta$ centers, which can be either intrinsically present or generated by the electrical stress applied to the SRO matrix [14].

Regarding the electrical behavior, two different electrical behaviors have been obtained from the red and blue LECs. **Figure 2** shows the current density (J) as a function of the electric field (E) of LECs working in accumulation mode (positive bias to the gate).

The S-LEC$_{30}$ shows a high current state (HCS) at low electric fields (<4 MV/cm), followed by a switch by the current to a low conduction state (LCS). Our group has observed this resistive switching (RS) from the HCS to LCS in previous studies and at both forward and reverse biases [14, 15, 19–21]. Such effect was related to the annihilation of conductive paths created by adjacent stable silicon nanoparticles (Si-nps) and unstable silicon nanoclusters (Si-ncls) in which Si-Si bonds can be broken creating some structural changes (defects), including some blue luminescent centers [15, 19, 20]. Recent reports regarding the same electrical switching in SRO films were observed, relating it to the presence of a conductive nanofilament [21–24]. Analysis of TEM imaging showed that the filament is created and annihilated by structural changes due to Joule heating effect produced by the high current flow, which allows the
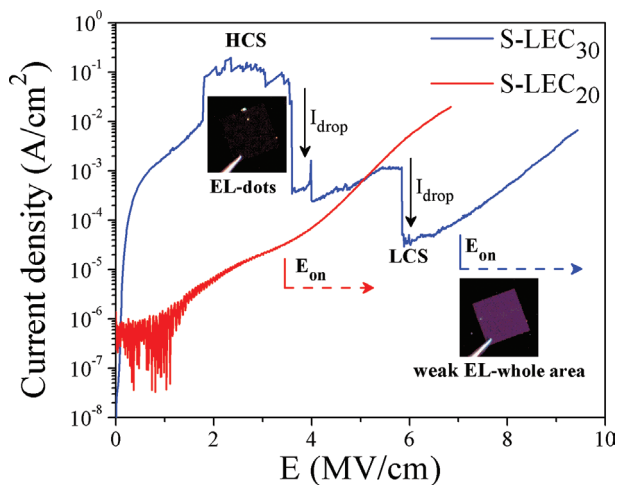

Figure 2. J-E curve from SRO$_{30}$- and SRO$_{20}$-based LECs. Insets are depicting images of EL dots and weak whole area EL.

crystallization (HCS) or amorphization (LCS) of the nanofilament [25]. These observations agree with our asseverations regarding the resistive switching observed in our S-LEC$_{30}$ [24]. During HCS regime, current jumps and drops corresponding to the appearance or disappearance of electroluminescent spots (EL dots) on the LEC surface have been observed (see inset in **Figure 3**) [14, 15, 19, 20]. Once the current fluctuations disappear, through an electrical annealing, the current behavior stabilizes allowing for the whole area EL [2, 14, 19].

On the other hand, the electrical behavior of most of LECs with SRO$_{20}$ films does not show current fluctuations. This effect has been related to the presence of well-separated Si-ncs and observed mainly on samples with a relatively high density of Si-nps [14]. This suggests that a denser network of conductive paths becomes more likely as the Si-ncs density increases, allowing for a uniform charge flow through the whole capacitor area.

In fact, it has been found that the trap-assisted tunneling (TAT) conduction mechanism, through a quasi-continuum of defect traps, predominates in the HCS in the S-LEC$_{30}$ devices, where the trap energy (ϕt) was estimated to be around 1.99 eV [14]. The TAT conduction mechanism has been reported in SRO-based devices where the RS phenomenon has been observed, in agreement with the observation of the devices reported in this work [24]. On the other hand, Poole-Frenkel (P-F) tunneling was found to be the most likely charge transport mechanism in the S-LEC$_{20}$ devices.

Although excellent results have been obtained from light emitting devices based on SRO with Ro = 20 and 30, the turn-on electric field (E_{on}) is still higher than desired. As an improvement strategy to obtain devices that emit in a wider range of wavelengths, and at lower E_{on}, multi-layer structures involving SRO$_{10}$, SRO$_{20}$, and SRO$_{30}$ layers have been designed and fabricated. As it has been shown, both SRO$_{20}$ and SRO$_{30}$ exhibit intense PL. On the other hand, SRO films with higher R_0 show lower PL intensity but better conductive characteristics [15, 26]. If the characteristics of each SRO film are preserved in a SRO ML structure, it is possible to improve the charge injection and luminescence properties of SRO-based LECs using the band-gap engineering by the Si-nc size modulation. Under this approach, the composition, structural,
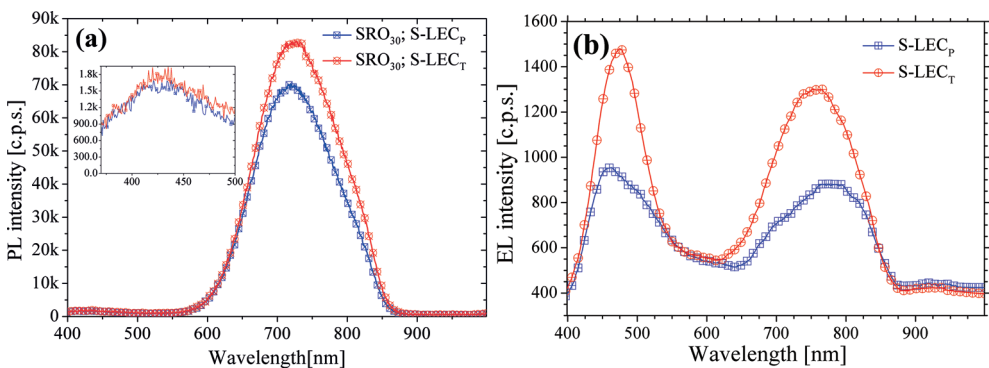

Figure 3. (a) PL spectra from SRO$_{30}$ films of S-LEC$_P$ and S-LEC$_T$. SRO films were excited with λ = 300 nm. (b) EL spectra for S-LEC$_P$ and S-LEC$_T$, when LECs were electrical polarized with 11.5 and 9.8 MV/cm.

and PL emission characteristics of SRO MLs with gradual change of R_0 from 10 to 30, and conversely, have been studied [27]. The Si and O gradual composition profiles in the $SRO_{10-20-30}$ multilayered system have been confirmed by X-ray photoelectron spectroscopy (XPS). The PL emission in these gradual SRO MLs increases when the emissive SRO layers (Ro = 20 and 30) are in the center of the ML. Moreover, the gradual Si-nc size according to the R_0 of each layer was preserved. Nevertheless, the study of the electro-optical characteristics of LECs with such scheme is still being carried out.

3.2. SRO monolayers on textured substrates

To evaluate the performance improvement of LECs on textured substrates (labeled as $S\text{-}LEC_T$), a SRO_{30} film with thickness of about 70 nm was used. The textured process was described in the experimental section. The SRO_{30} film was also deposited on a regular polished substrate, as a reference device, labeled as $S\text{-}LEC_P$. In both cases, the substrate was a P-type silicon wafer with resistivity between 2 and 4 $\Omega \times$ cm. Over the SRO, a 250-nm thick square gate of poly layer with an area of 1.54 mm^2 was deposited and defined. **Table 1** summarizes characteristics of both S-LECs.

Figure 3(a) shows the PL spectra of the SRO_{30} film present in the S-LECs. Roughening does not appear to significantly affect the emission properties of the active material when it is optically stimulated, as previously demonstrated [28, 29]. As can be observed, there are two peaks, one centered at 725 nm (red band) and a much weaker one at 428 nm (blue band, shown in the inset of **Figure 3(a)**). The emission in blue band is ascribed to non-bridging oxygen defects and oxygen deficiency-related centers [14, 30–34], whereas the red band is attributed to oxygen vacancies caused by the Si excess (720 to 740 nm) [31–33], as well as to interfacial defects in boundaries of silicon nanoclusters with the silicon oxide matrix (810 nm) [35–37].

Figure 3(b) exhibits the EL spectra of the S-LECs. Both LECs show two bands as well: blue and red, as PL. This indicates that PL and EL have the same origin, mainly attributed to SRO-related defects [25, 34, 37]. Since in this case the samples are electrically pumped, electrons are driven through deeper traps, allowing for a larger amount of radiative transitions of higher energy, such that emission in the blue band has comparable intensities to those of the red one. This phenomenon is not observed in PL due to its lower energetic source (UV radiation). $S\text{-}LEC_T$ reached a higher EL intensity than $S\text{-}LEC_P$. Additionally, $S\text{-}LEC_T$ requires less electrical power than $S\text{-}LEC_P$ to achieve its maximum intensity.

Figure 4 displays the J vs. E curve for both textured and non-textured LECs. The J-E curve exhibits the behavior of S-LECs for positive voltage, condition in which EL is observed. Under

ID	Texturing	Roughness [nm]	Peak density [cm^{-2}]	SRO_{30} thickness [nm]
$S\text{-}LEC_P$	No	0.5	0	65.9 ± 0.4
$S\text{-}LEC_T$	Yes	4.0 ± 0.2	3.7 ± 1.8 × 10^{10}	68.8 ± 1.7

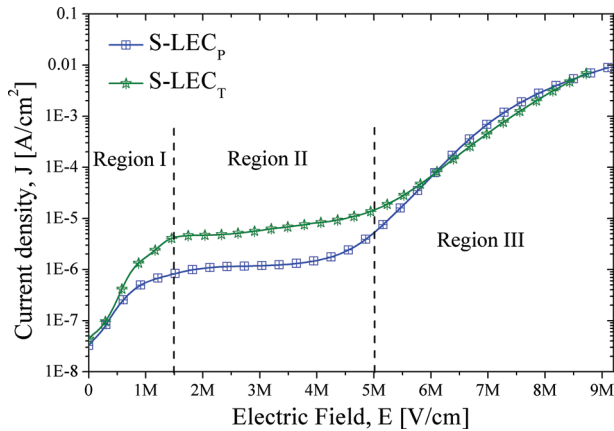**Table 1.** Roughening features and SRO_{30} thickness of $S\text{-}LEC_P$ and $S\text{-}LEC_T$.

Figure 4. Current density as a function of electric field of S-LECs. Curves are divided in three regions, according to the conduction mechanism for each E range.

this condition, an inversion layer is formed in the SRO/Si-substrate interface. S-LECs presented in this section did not show current jumps, neither the RS from HCS to a LCS, contrary to other reports [14, 15, 19–24]. At low electric fields (region I), the ohmic conduction mechanism dominates the carrier transport; however, roughening of the substrate surface in S-LEC$_T$ propitiates a current increase due to the conical structures in silicon surface, which act as tips highly populated by electrons allowing for higher injection rates through the SRO layer. At medium electric fields (region II), the Fowler-Nordheim tunneling mechanism is responsible for the conduction. In this regimen, the observed current offset between curves of S-LECs is due to the augment of current density at lower electric fields; however, both curves present comparable slope [28]. At the higher electric fields (region III), the trap-assisted tunneling mechanism controls the carrier transport. In this regimen, both S-LEC$_P$ and S-LEC$_T$ present electroluminescence, in agreement with results of the LECs presented in Section 3.1. As can be seen in **Figure 4**, in region III the J-E curves of S-LECs overlap, but even though they have similar electrical responses, S-LEC$_T$ achieves a substantial improvement of electro-optical properties as compared to its counterpart, as it will be shown later.

3.3. SRO multilayers

LECs based on multilayered structures are obtained by a multistep deposition process. While the samples remain in the reactor, the LPCVD system is periodically adjusted to change the R_0, modifying the silicon excess in the layer deposited during each period. Two structures were fabricated: M-LEC$_{525}$ and M-LEC$_{1025}$, which alternate four mainly conductive layers ($R_0 = 5$) with three primarily emitting layers ($R_0 = 25$). For both devices, P-type silicon wafers with resistivity between 2 and 4 $\Omega \times$ cm were used as substrate.

M-LEC$_{525}$ has SRO$_5$ as conductive layer and SRO$_{25}$ as emitting layer, with thickness of 15 and 25 nm, respectively. Meanwhile, M-LEC$_{1025}$ uses the same material for emitting layers but

SRO_{10} instead of SRO_5, with thickness of 10 nm. The nominal thickness of the whole structure is 115 nm approximately. In the top of the multilayer, a semitransparent 250 -nm thick n$^+$ poly-crystalline silicon layer was deposited, and a square gate with an area of 4.05 mm^2 was formed.

Figure 5(a) shows the PL spectra of the SRO multilayers. Two bands are observed: blue and red bands. The shape of PL spectra is quite similar to that of SRO_{30}, which does not have Si-ncs [25], suggesting that, as in SRO_{30}, oxygen defects in the oxide matrix due to the silicon excess are the main cause of PL emission in multilayered structures [34]. As it is reported in [37], Si-ncs are observed in SRO multilayers, and their size and density depend on the features of each layer (silicon excess, thickness, etc.), in agreement with other reports on multilayers [27, 34, 38]. **Table 2** summarizes the Si-nc features of M-LECs. **Figure 5(b)** and **(c)** displays the EL spectra of M-LECs. Again, two luminescent bands are obtained; however, M-LEC$_{525}$ has a more prominent blue band, whereas M-LEC$_{1025}$ achieves higher emission in red band. In [37], this difference is associated with the size and density of Si-ncs embedded in the conductive layers. In M-LEC$_{525}$, SRO_5 layers allow electrons reach deeper traps (blue emission centers); meanwhile M-LEC$_{1025}$ requires higher electric fields (energy) in order to excite the same emission centers. Thus, conductive layers with bigger size and lower density of Si-ncs produce
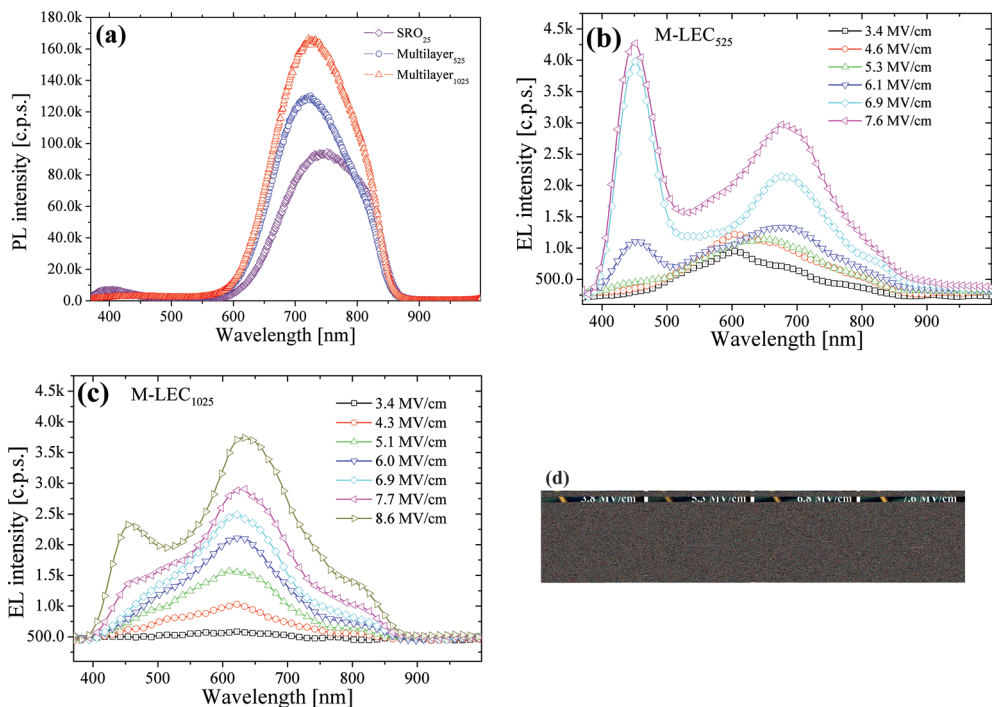

Figure 5. (a) PL spectra of SRO multilayers of M-LECs. SRO mono- and multilayers were excited with λ = 300 nm. EL spectra of (b) M-LEC$_{525}$ and (c) M-LEC$_{1025}$. (d) EL emission of M-LEC$_{525}$ for different electric fields. Note that whole area emission and localized bright spots can coexist.

ID	Si-nc size of CL[*] [nm]	Si-nc density in CL [cm³]	Si-nc size of EmL[**] [nm]	Si-nc density in EmL [cm³]	Nominal thickness [nm]
M-LEC$_{525}$	4.0	1.06×10^{12}	2.1	5.76×10^{11}	131.1 ± 7.6
M-LEC$_{1025}$	3.6	1.30×10^{12}	1.8	7.43×10^{11}	116.7 ± 1.6

[*]CL—conductive layer.

[**]EmL—emitting layer.

Table 2. Size and density of Si-nc in each layer, as well as nominal thickness of multilayered structure.

M-LECs with brightest blue emission at lower electric fields. **Figure 5(d)** shows digital pictures of the EL emission of M-LEC$_{525}$ biased with different electric fields, where blue color is predominant in the emission.

Figure 6 exhibits J-E characteristics of the M-LECs. In a first test, M-LECs present a LCS, but once they reach a high electric field (E > 5 MV/cm), M-LECs change to a HCS and remain in this regimen for the subsequent measurements, as previously reported in [39] and agreeing with others works [34, 40]. During first current-voltage measurement, Si-ncs are ordered forming conductive trajectories (electroforming) whereby electrons can be easily driven through the SRO multilayers [22, 23]. Across their conductive path, they can impact other electrons not only increasing the current density but also augmenting the number of electrons able to decay at different trap levels, enhancing the emission intensity as well. In [39], it is reported that thermionic emission, Poole-Frenkel, trap-assisted tunneling, and impact ionization conduction mechanisms are responsible for the charge transport. The first two dominate conduction in low (E < 2 MV/cm) and medium (2 MV/cm < E < 4 MV/cm) electric field regimes, respectively. Meanwhile, TAT and impact ionization are responsible for charge transport in
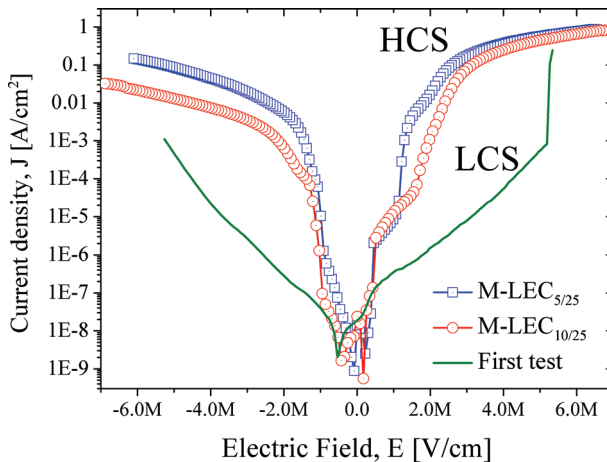

Figure 6. Current density as a function of electric field for M-LECs. In a first sweep, M-LECs present a LCS, but once they achieve a HCS, LECs preserve this behavior maintaining EL emission.

high-energy regime, which is also the region where brightest EL is observed. For E < 6 MV/cm, only TAT mechanism is presented, but once electric field overpass 6 MV/cm, impact ionization takes place, increasing substantially the EL intensity.

4. Discussion

Figure 7(a) and **(b)** shows, respectively, the normalized PL spectra and the J-E curve for S-LEC$_P$, S-LEC$_{TI}$, M-LEC$_{525}$, and M-LEC$_{1025}$ in order to compare single- and multilayer-based LECs. Regarding PL response, multilayer of M-LEC$_{1025}$ records the highest intensity, followed by M-LEC$_{525}$ and single SRO$_{25}$ and SRO$_{30}$ layers. The total PL emission in a multilayered structure has two contributions: emission of SRO$_{25}$ layers, which is the main contribution, and emission from the conductive SRO layers (SRO$_5$ or SRO$_{10}$), which have a smaller contribution [37]. As reported in [26], SRO films with higher density of Si-ncs with size lower than 3 nm have the brighter emission. In these films, defects are formed at the interface between SRO and the Si-ncs, acting as localized states from where electrons decay through ground states, emitting light in the process. Even though conductive SRO layers mainly enhance electrical characteristics in M-LECs, the presence of Si-ncs into SiO$_x$ matrix propitiates a non-negligible contribution to PL emission, and as can be observed in **Table 2**, the highest density with the lowest size of Si-ncs is achieved in M-LEC$_{1025}$, in agreement with PL response.

In **Figure 7(b)**, J-E curves of LECs are presented. A substantial augment of current density in M-LECs with respect to that one in S-LECs can be observed. M-LECs reach the HCS at lower voltages. This improvement of carrier transport in M-LECs is ascribed to the high silicon content in SRO conductive layers. In the electroforming process observed in these M-LECs, which occurs in the first J-E measurement, Si-ncs are connected creating multiple preferential conductive paths between the poly and Si-substrate. Electrons can easily flow through those conductive trajectories in SRO MLs improving the current density. Regarding S-LECs, SRO layer does not have Si-ncs to form conductive paths; however, it has a high density of defects.
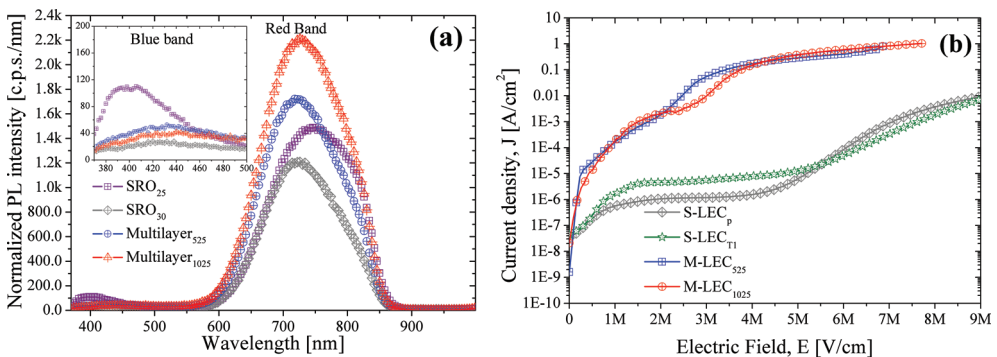

Figure 7. (a) PL spectra normalized with respect to thickness of the SRO single or multilayer. (b) Current density as a function of electric field for S-LECs and M-LECs.

This high content of defects allows that electron transit by a sequence of low energetic traps through the SRO film, named as low resistive trajectories. Even though these trajectories are low resistive, the charge-trapping effect still takes place, such that enhancement of current density is limited and a HCS is not reached. Fabricating S-LECs on textured substrate allow improvement of carrier injection to the SRO film; however, this technique also has results with lower current density improvement than those in a multilayered structure.

Figure 8 displays the integrated EL intensity as a function of electric field for (a) S-LECs on polished substrates and (b) S-LECs on textured substrate and M-LECs. These figures allow comparing LECs by means of two figures of merit: turn-on electric field (E_{on}) and the operation range. The E_{on} is the electric field needed for the EL intensity to overpass the noise level and begin to rise; meanwhile, the operation range is the electric field range in which LECs emit light without electrical damage, and it must go from E_{on} to an E value before dielectric breakdown.

As it can be seen in **Figure 8(a)**, S-LEC$_{20}$ (devices that emit in red) operate on a greater range (from 3.7 to 6 MV/cm) than S-LEC$_{30}$ (devices that emit in blue), which works from 7.0 to 8.3 MV/cm, approximately. The electric field range where it was possible to register EL spectra for S-LEC$_{30}$ is 7.1–8.3 MV/cm and for S-LEC$_{20}$ is 3.7–5.7 MV/cm. As can be noted, a larger electric field is required to obtain the blue emission as compared to the red one. In accordance, the devices without Si-ncs into SRO films and emitting in blue wavelengths require a larger electric field (E > 7MV/cm) to turn on. Additionally, a nearly linear fitting was done to the experimental data. The slope found for each device is slightly different, suggesting that the mechanisms responsible of the EL increase are not the same. A quite similar conclusion was obtained in Section 3.1, where EL emission is observed when TAT and P-F mechanisms dominate the charge transport in S-LEC$_{30}$ and S-LEC$_{20}$, respectively.

In **Figure 8(b)**, it is found that the operation range of S-LEC$_P$ and S-LEC$_T$ is from 8.5 to 11.5 MV/cm and from 7 to 10 MV/cm, respectively. These operation ranges are lower than that one of M-LECs, which have an operation range from 3 to 9 MV/cm, approximately. Thus, M-LECs
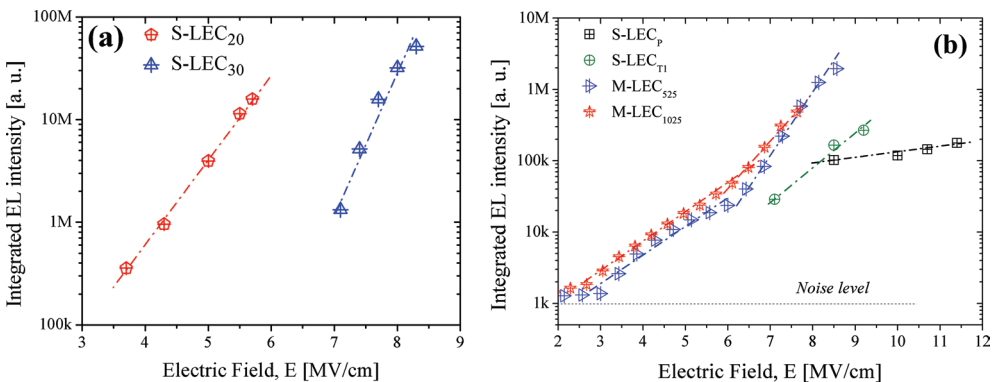

Figure 8. Integrated EL intensity as a function of electric field for (a) single-layer LECS and (b) single-layer LECs on textured substrate and M-LECs. Noise level is used as reference to evaluate EL emission of LECs. Intensities of graph (a) are not comparable with graph (b) because of differences in setup and testing condition.

ID	Voltage [V]	E [MV/cm]	Current [μA]	P_e [mW]	P_{opt} [μW]	η_c [10^{-4} %]
S-LEC$_P$	80	11.4	113	9.04	0.17	18.7
S-LEC$_{T1}$	68	9.7	78	5.30	0.34	64.1
M-LEC$_{525}$	95	7.3	30×10^3	2.85×10^3	2.75	1.0
M-LEC$_{1025}$	95	8.2	37×10^3	3.52×10^3	2.71	0.9

Table 3. Voltage, electric field, electrical power, optical power, and conversion efficiency of LECs: single layer, roughening substrate, and multilayers.

have twice higher operation range than S-LECs. Moreover, the E_{ON} value of M-LECs is lower than that one of S-LECs, and the EL intensity of M-LECs gradually increases as the electric field becomes stronger. In contrast, S-LECs require a higher electric field to emit light, and their transition from turn-off state to turn-on state is abrupt. Hence, M-LECs are better candidates to be integrated in all-silicon photonic circuits due to the lower E_{on} and a wider operation range.

Finally, the conversion efficiency (η_c) is analyzed for each device. The η_c is defined as the ratio of the optical power (P_{opt}) with respect to the electrical power (P_e). The latter power is calculated as $P_e = V*I$, where V is the voltage and I is the electrical current in which a specific P_{opt} is measured. **Table 3** resumes values of voltage, electrical current, P_e, P_{opt}, and conversion efficiency (η_c) of LECs with the different strategies used. These parameters were selected considering the best electro-optical performance. As we can see, the S-LECs are more efficient but have lower values of P_{opt}, while M-LECs are less efficient but achieve a significantly higher P_{opt}. Based only on efficiency and without considering the application, S-LECs would be the best option; however, as is aforementioned, M-LECs have other advantages over S-LECs. A higher operation range, lower E_{on} values, an EL intensity that gradually increases, and a greater P_{opt} are the features that place M-LECs as the best option to be integrated in all-silicon photonic circuit. In [4], it has been demonstrated that S-LECs are enough to guaranty the functionality of all-silicon photonic circuits; however, the LECs operate close to the noise level. Thus, the performance of such system could be improved using M-LECs, which have enhanced electro-optical characteristics.

5. Conclusion(s)

This work was focused on the different strategies used to improve the performance of SRO-based LECs fully compatible with the CMOS technology to be integrated in an all-silicon photonic circuit. We reviewed the fabrication and characterization of LECs that use different substrate treatments and a variety of SRO compositions and configurations. LECs were fabricated with single SRO layers (S-LECs) deposited on polished and textured Si substrates. LECs with SRO in a multilayered structure (M-LECs) involving a conductive SRO layer with an emitting one were also fabricated.

It was found that M-LEC$_{1025}$ emits the highest PL intensity, followed by M-LEC$_{525}$ and finally those with single SRO$_{25}$ and SRO$_{30}$ layers. An improved charge injection observed through

an augment of current density was obtained in M-LECs with respect to S-LECs, even though S-LECs use textured silicon substrate to improve carrier injection. M-LECs achieve high conduction state with lower voltages, which is ascribed to the high silicon content in SRO conductive layers, forming conductive trajectories by means of electrons that are easily driven through multilayers.

The electro-optical characterization of different LECs exhibited that M-LECs have twice higher operation range than S-LECs. Moreover, M-LECs emit at lower electric fields and their intensity gradually increases as the electric field becomes stronger. In the opposite, S-LECs require a high electric field to emit light, and their transition from turn-off state to turn-on state is abrupt. Hence, M-LECs perform a better behavior to be integrated in all-silicon photonic circuits based on a lower E_{on} and wider operation range. A higher operation range, lower E_{on}, EL emission that gradually increase, and a greater P_{opt} are the features that place M-LEC as the best option to be integrated in all-silicon photonic circuit.

Acknowledgements

Conflict of interest

Authors declare that there is no conflict of interest.

Author details

Jesús Alarcón-Salazar[1], Liliana Palacios-Huerta[1], Alfredo Abelardo González-Fernández[1], Alfredo Morales-Sánchez[2]* and Mariano Aceves-Mijares[1]*

*Address all correspondence to: alfredo.morales@cimav.edu.mx and maceves@inaoep.mx

1 Electronics Department, National Institute of Astrophysics Optics and Electronics, Tonantzintla, Puebla, Mexico

2 Advanced Materials Research Center (CIMAV), Monterrey-PIIT, Apodaca, Nuevo Leon, Mexico

References

[1] Muñoz P, Micó G, Bru L, Pastor D, Pérez D, Doménech J, Fernández J, Baños R, Gargallo B, Alemany R, Sánchez A, Cirera J, Mas R, Domínguez C. Silicon nitride photonic

integration platforms for visible, near-infrared and mid-infrared applications. Sensors. 2017;**17**(9):2088. DOI: 10.3390/s17092088

[2] Fernández AAG, Mijares MA, Sánchez AM, Leyva KM. Intense whole area electroluminescence from low pressure chemical vapor deposition-silicon-rich oxide based light emitting capacitors. Journal of Applied Physics. 2010;**108**(4):43105. DOI: https://doi.org/10.1063/1.3465335

[3] Alarcón-Salazar J, Zaldívar-Huerta IE, Aceves-Mijares M. An optoelectronic circuit with a light source, an optical waveguide and a sensor all on silicon: Results and analysis of a novel system. Optics & Laser Technology. 2016;**84**:40-47. DOI: https://doi.org/10.1016/j.optlastec.2016.04.013

[4] González-Fernández AA, Juvert J, Aceves-Mijares M, Domínguez C. Monolithic integration of a silicon-based photonic transceiver in a CMOS process. IEEE Photonics Journal. 2016;**8**(1):1-13. DOI: 10.1109/JPHOT.2015.2505144

[5] Dong DRYD, Irene EA. Preparation and some preparation and some properties of chemically vapor-deposited Si-rich SiO and SigN, films D. Journal of the Electrochemical Society (JES) and the ECS Journal of Solid State Science and Technology. 1977;**5**:819-823. DOI: doi: 10.1149/1.2131555

[6] Alarcón-Salazar J, López-Estopier R, Quiroga-González E, Morales-Sánchez A, Pedraza-Chávez J, Zaldívar-Huerta IE, Aceves-Mijares M. Silicon-Rich oxide obtained by low-pressure chemical vapor deposition to develop silicon light sources. In: Sudheer Neralla, editor. Chemical Vapor Deposition - Recent Advances and Applications in Optical, Solar Cells and Solid State Devices. InTech; 2016. DOI: 10.5772/63012. http://dx.doi.org/10.5772/63012

[7] Ogudo KA, Schmieder D, Foty D, Snyman LW. Optical propagation and refraction in silicon complementary metal-oxide-semiconductor structures at 750 nm: Toward on-chip optical links and microphotonic systems. Journal of Micro/Nanolithography, MEMS, and MOEMSournal of Micro/Nanolithography, MEMS, and MOEMS. 2013;**12**(1):13015. DOI: 10.1117/1.JMM.12.1.013015

[8] Xu K, Ning N, Ogudo KA, Polleux J-L, Yu Q, Snyman LW, Light emission in silicon: From device physics to applications. In: Proceedings of the SPIE 9667, International Workshop on Thin Films for Electronics, Electro-Optics, Energy, and Sensors. 2015:966702-1-966702-10. https://doi.org/10.1117/12.2199841

[9] Misiakos K, Petrou PS, Kakabakos SE, Yannoukakos D, Contopanagos H, Knoll T, Nounesis G. Fully integrated monolithic optoelectronic transducer for real-time protein and DNA detection: The NEMOSLAB approach. Biosensors and Bioelectronics. 2010;**26**(4):1528-1535. DOI: https://doi.org/10.1016/j.bios.2010.07.104

[10] Camacho-Aguilera RE, Cai Y, Patel N, Bessette JT, Romagnoli M, Kimerling LC, Michel J. An electrically pumped germanium laser. Optics Express. 2012;**20**(10):11316. DOI: https://doi.org/10.1364/OE.20.011316

[11] Sun C, Wade MT, Lee Y, Orcutt JS, Alloatti L, Georgas MS, Waterman AS, Shainline JM, Avizienis RR, Lin S, Moss BR, Kumar R, Pavanello F, Atabaki AH, Cook HM, Ou AJ, Leu JC,

Chen Y-H, Asanović K, Ram RJ, Popović MA, and Stojanović VM. Single-chip micro-processor that communicates directly using light. Nature. 2015;**528**(7583):534-538. DOI: https://doi.org/10.1038/nature16454

[12] Gonzalez-Fernandez AA, Liles AA, Persheyev S, Debnath K, O'Faolain L. Wavelength-controlled external-cavity laser with a silicon photonic crystal resonant reflector. In: Schröder H, Chen RT, editors. Proc. SPIE 9753, Optical Interconnects XVI, San Francisco, California. 2016. pp. 975317. DOI: https://doi.org/10.1117/12.2213288

[13] Jambois O, Berencen Y, Hijazi K, Wojdak M, Kenyon AJ, Gourbilleau F, Rizk R, Garrido B. Current transport and electroluminescence mechanisms in thin SiO2 films containing Si nanocluster-sensitized erbium ions. Journal of Applied Physics. 2009;**106**(6):063526-063532. DOI: https://doi.org/10.1063/1.3213386

[14] Palacios Huerta L, Cabañas Tay SA, Luna López J-A, Aceves M, Coyopol A, Morales-Sánchez A. Effect of the structure on luminescent characteristics of SRO-based light emitting capacitors. Nanotechnology. 2015;**26**(39):395202. DOI: https://doi.org/10.1088/0957-4484/26/39/395202

[15] Morales-Sánchez A, Monfil-Leyva K, González AA, Aceves-Mijares M, Carrillo J, Luna-López JA, Domínguez C, Barreto J, Flores-Gracia FJ. Strong blue and red luminescence in silicon nanoparticles based light emitting capacitors. Applied Physics Letters. 2011;**99**:171102. DOI: https://doi.org/10.1063/1.3655997

[16] Lai BH, Cheng CH, Lin GR. Electroluminescent wavelength shift of Si-rich SiOx based blue and green MOSLEDs induced by O/Si composition Si-QD size variations. Optical Materials Express. 2013;**3**(2):166. DOI: https://doi.org/10.1364/OME.3.000166

[17] Wang DC, Chen JR, Zhu J, Lu C-T, Lu M. On the spectral difference between electro-luminescence and photoluminescence of Si nanocrystals: A mechanism study of electroluminescence. Journal of Nanoparticle Research. 2013;**15**(11):2063. DOI: https://doi.org/10.1007/s11051-013-2063-x

[18] Chen D, Xie ZQ, Wu Q, Zhao YY, Lu M. Electroluminescence of Si nanocrystals-doped SiO$_2$. Chinese Physics Letters. 2007;**24**(8):2390. DOI: https://doi.org/10.1088/0256-307X/24/8/064

[19] Morales-Sánchez A, Barreto J, Domínguez C, Aceves M, Luna-López JA. The mechanism of electrical annihilation of conductive paths and charge trapping in silico- rich oxides. Nanotechnology. 2009;**20**(4):045201. DOI: https://doi.org/10.1088/0957-4484/20/4/045201

[20] Morales-Sánchez A, Barreto J, Domínguez C, Aceves-Mijares M, Luna-López JA, Perál-varez M, Garrido B. DC and AC electroluminescence in silicon nanoparticles embed-ded in silicon-rich oxide films. Nanotechnology. 2010;**21**(8):085710. DOI: https://doi.org/10.1088/0957-4484/21/8/085710

[21] Yao J, Sun Z, Zhong L, Natelson D, Tour JM. Resistive switches and memories from sili-con oxide. Nano Letters. 2010;**10**(10):4105. DOI: 10.1021/nl102255r

[22] Yao J, Zhong L, Natelson D, Tour JM. In situ imaging of the conducting filament in a silicon oxide resistive switch. Scientific Reports. 2012;**2**(242):1-5. DOI: 10.1038/srep00242

[23] Mehonic A, Vrajitoarea A, Cueff S, Hudziak S, Howe H, Labbé C, Rizk R, Pepper M, Kenyon AJ. Quantum conductance in silicon oxide resistive memory devices. Scientific Reports. 2013;**3**:2708. DOI: 10.1038/srep02708

[24] Mehonic A, Cueff S, Wojdak M, Hudziak S, Labbé C, Rizk R, Kenyon A. Electrically tailored resistance switching in silicon oxide. Nanotechnology. 2012;**23**(45):455201. DOI: https://doi.org/10.1088/0957-4484/23/45/455201

[25] Aceves-Mijares M, González-Fernández AA, López-Estopier R, Luna-López A, Berman-Mendoza D, Morales A, Falcony C, Domínguez C, Murphy-Arteaga R. On the origin of light emission in silicon rich oxide obtained by low-pressure chemical vapor deposition. Journal of Nanomaterials. 2012;**2012**:890701. DOI: http://dx.doi.org/10.1155/2012/890701

[26] Morales-Sánchez A, Barreto J, Domínguez-Horna C, AcevesMijares M, Luna López JA. Optical characterization of silicon rich oxide films. Sensors and Actuators A. 2008;**142**:12-18. DOI: https://doi.org/10.1016/j.sna.2007.03.008

[27] Palacios Huerta L, Cabañas-Tay SA, Cardona Castro MA, Aceves Mijares M, Domínguez Horna C, Morales Sánchez A. Structural and optical properties of silicon rich oxide films in graded-stoichiometric multilayers for optoelectronic devices. Applied Physics Letters. 2016;**109**:031906. DOI: https://doi.org/10.1063/1.4959080

[28] Alarcón-Salazar J, Vásquez-Agustín MA, Quiroga-González E, Zaldívar-Huerta IE, Aceves-Mijares M. Comparison of light emitting capacitors with textured and polished silicon substrates towards the understanding of the emission mechanisms. Submitted to Journal of Luminescence. 2018 (under review)

[29] Alarcón-Salazar J. Analysis, design, fabrication and characterization of the essential devices to integrate an all-silicon photonic circuit [PhD thesis]. INAOE, Puebla, México. April 2017. DOI: http://inaoe.repositorioinstitucional.mx/jspui/handle/1009/343

[30] Spallino L, Vaccaro L, Sciortino L, Agnello S, Buscarino G, Cannas M, Mario Gelardi F. Visible-ultraviolet vibronic emission of silica nanoparticles. Physical Chemistry Chemical Physics. 2014;**16**:22028-22034. DOI: 10.1039/c4cp02995j

[31] Sopinsky M, Khomchenko V. Electroluminescence in SiO_x films and SiO_x-film-based system. Current Opinion in Solid State & Materials Science. 2003;**7**:97-109. DOI: https://doi.org/10.1016/S1359-0286(03)00048-2

[32] López-Estopier R, Aceves-Mijares M, Falcony C. Cathodo- and photo-luminescence of silicon rich oxide films obtained by LPCVD. In: Yamamoto N, editor. Cathodoluminescence. InTech; 2012. pp. 253-272. DOI: 10.5772/34888

[33] Kalnitsky A, Ellul JP, Poindexter EH, Caplan PJ, Lux RA, Boothroyd AR. Rechargeable E' centers in silicon implanted SiO_2 films. Journal of Applied Physics. 1990;**67**(12):7359-7367. DOI: https://doi.org/10.1063/1.346059

[34] Wang M, Anopchenko A, Marconi A, Moser E, Prezioso S, Pavesi L, Pucker G, Bellutti P, Vanzetti L. Light emitting devices based on nanocrystalline-silicon multilayer structure. Physica E. 2009;**41**:912-915. DOI: https://doi.org/10.1016/j.physe.2008.08.009

[35] Quiroga-González E, Bensch W, Aceves-Mijares M, Yu Z, López-Estopier R, Monfil-Leyva K. On the photoluminescence of multilayer arrays of silicon rich oxide with high silicon content prepared by low pressure chemical vapor deposition. Thin Solid Films. 2014;**519**:8030-8036. DOI: https://doi.org/10.1016/j.tsf.2011.06.020

[36] Vinciguerra V, Franzo G, Priolo F, Iacona F, Spinella C. Quantum confinement and recombination dynamics in silicon nanocrystals embedded in Si/SiO$_2$ superlattices. Journal of Applied Physics. 2000;**87**:8165. DOI: https://doi.org/10.1063/1.373513

[37] Alarcón-Salazar J, Zaldívar-Huerta IE, Morales-Sánchez A, Domínguez C, Pedraza-Chávez J, Aceves-Mijares M. Enhancing emission and conduction of light emitting capacitors by multilayered structures of silicon rich oxide. Sensors and Actuators A. 2017;**265**:306-312 http://dx.doi.org/10.1016/j.sna.2017.08.047

[38] Limpens R, Lesage A, Fujii M, Gregorkiewicz T. Size confinement of Si nanocrystals in multinanolayer structures. Scientific Reports. 2015;**5**(17289). DOI: 10.1038/srep17289

[39] Alarcón-Salazar J, Zaldívar-Huerta IE, Aceves-Mijares M, Electrical and electroluminescent characterization of nanometric multilayers of SiO$_X$/SiO$_Y$ obtained by LPCVD including non-normal emission. Journal of Applied Physics. 2016;**119**(21):215101. DOI: https://doi.org/10.1063/1.4952730

[40] Fu S-W, Chen H-J, Wu H-T, Shih C-F. Effect of SiO$_2$ layers on electroluminescence from Si nanocrystal/SiO$_2$ superlattices prepared using argon ion beam assisted sputtering. Vacuum. 2016;**126**:59-62. DOI: https://doi.org/10.1016/j.vacuum.2016.01.020